COBEM 2021 26th International Congress of Mechanical Engineering
November 22-26, 2021, Virtual Congress, Brazil
ABCM Associação Brasileira de Engenharia e Ciências Mecânicas

COB-2021-0429
Vibration Analysis of a Quadcopter Carrying a Payload

Renan Sanches Geronel
São Paulo State University (UNESP), School of Engineering of Ilha Solteira, Ilha Solteira-SP Brazil
renan.sanches@unesp.br

Ruxandra Mihaela Botez
École de Technologie Supérieure (ETS), Quebec University , Montreal Canada
ruxandra.botez@etsmtl.ca

Douglas Domingues Bueno
São Paulo State University (UNESP), School of Engineering of Ilha Solteira, Ilha Solteira-SP Brazil
douglas.bueno@unesp.br

Abstract: *Unmanned Aerial Vehicles (UAVs) have been conquering continuous importance due to their variety of applications. Most of them present an additional load attached to the UAV, such as sensors, measurement tools, and fragile loads, requiring great stability to transport safely the payload and work accurately. The interest of this article is to evaluate the impact of the vibration on the dynamic modeling of a UAV carrying a payload. External disturbances and maneuvers can create undesired vibration to components, influencing directly the system behavior and the UAV trajectory. The controller based on Sliding Mode Control is designed to guarantee a safe trajectory, while the State-Feedback Control is used to attenuate the oscillation displacement (between the UAV and its payload), when a flexible attachment is considered. Therefore, designing a robust controller can improve the UAV performance and reduce the interference on the payload and onboard components.*

Keywords: *Unmanned Aerial Vehicle, Sliding Mode Control, State-Feedback Control, Payload Vibration*

1. INTRODUCTION

Advances in technology and costs reduction have led to increasing the use of Unmanned Aerial Vehicles (UAVs) by medical field, monitoring environment, food and products transportation, and other applications Kuitche and Botez (2019). Their use is mainly motivated to overcome some geographical and logistics challenges due to the poor infrastructure of low income countries. The UAVs present the ability to carry several sensors and fragile payload, and depending on the level of vibration caused by external disturbances, propellers rotation, trajectories and maneuvers, the quality of the onboard signal or payload integrity can be negatively impacted Yañez-Badillo *et al.* (2019a) and Dancila and Botez (2021). In the medical field, organs and pharmaceutical goods might deteriorate during a flight when they are affected by unwanted vibration, since the tissues are fragile and some medical products may lose their therapeutic effect Yakushiji *et al.* (2020).

UAVs have been conquering great importance in the medical field since they might reduce costs and overpass logistic challenges (traffic jams, inaccessible roads, delivery time). However, these applications have been widely studied to evaluate the influence of aerial transportation on the loads. Hii *et al.* (2019) investigated the effects of temperature and vibration on insulin during a UAV transportation. A significant and continuous perturbation can cause irreversible aggregation on insulin, and then its disposal be necessary. Hampson (2018) used a commercial drone to explore the feasibility of kidney transportation. A smart cooler was attached directly to the UAV body, and several sensors (temperature, pressure, vibration) are located with the organ for monitoring the kidney quality over the proposed flight. The experiment aimed to evaluate the safe boundaries of vibration that the kidney could be subjected to. In addition, the delivery time is crucial, since the longer the organ takes to be translated into a recipient, the poorer the organ functions afterward.

The use of a robust controller might assure the improvement of the UAV performance. Depending on the proposed trajectory, an undesired vibration can be created from the UAV to its payload. Overall, the generic control for a quacopter is composed of two loops: the inner loop that is responsible for the UAV attitude, and the outer loop, in which is able to guide the UAV to during the desired path. Several strategies have been proposed to design the controller, such as Proportional Integral Derivative (PID) Kammegne *et al.* (2017), Sate Feedback Rahmani *et al.* (2021) and Sliding Mode Control (SMC) Sudhir and Swamp (2016).

External disturbances effects might also increase the unwanted vibration on the UAV and its payload Ghazi *et al.* (2021). Alkomy and Shan (2021) investigated the vibration influence on the cable-suspended payload during a flight.

Polynomial trajectory technique was addressed to create smooth trajectories, and then reducing the transmitted vibration from the quadcopter to its payload regardless the chosen path. Additionally, the influence of external disturbances can impact directly the UAV Yañez-Badillo *et al.* (2019b) and its payload performance Aouf *et al.* (2000). Then, the reduction of unwanted oscillation and external disturbances can improve the UAV performance and its payload integrity.

In this context, this article aims to evaluate the undesired vibration transmitted from the quadcopter to its payload during a flight, and under external disturbances. The equations of motion for a UAV carrying a payload have been presented, assuming a flexible attachment between them. Since unwanted vibration can decrease the UAV performance, the Sliding Mode Control is designed to track the quadcopter trajectory, while the State-Feedback Control (H_∞) is used to attenuate the residual oscillations on the payload. Therefore, the combination of these strategies can lead safely the UAV over the desired path, as well as to attenuate the external perturbation and undesired oscillations, guaranteeing a safe transportation of fragile goods by the UAV.

2. METHODOLOGY

The quadcopter dynamics are generally represented in two coordinate reference frames: inertial and body. In the body-reference frame, it is represented the linear and angular velocities, while in the inertial reference frame is defined the orientation and attitude of the quadcopter. The equations of motion govern the UAV behavior under specific conditions according to the modeling hypothesis. These position and orientation vectors, references and principles are widely addressed in literature by Fossen (1999) and Gobeaut *et al.* (2009).

2.1 Dynamic model

For the proposed model, the system is composed of a UAV and a vibrating payload. The connection between the UAV and its payload is assumed to be an elastic link. At this connection point (as seen in Fig. 1), there are three components (F_x, F_y and F_z) that are responsible to keep the payload attached safely during the flight. Therefore, based on the UAV maneuvers and external disturbances, these forces can impact severely the payload, affecting its integrity. Fig. 1 depicts the schematic illustration of the UAV with its payload.

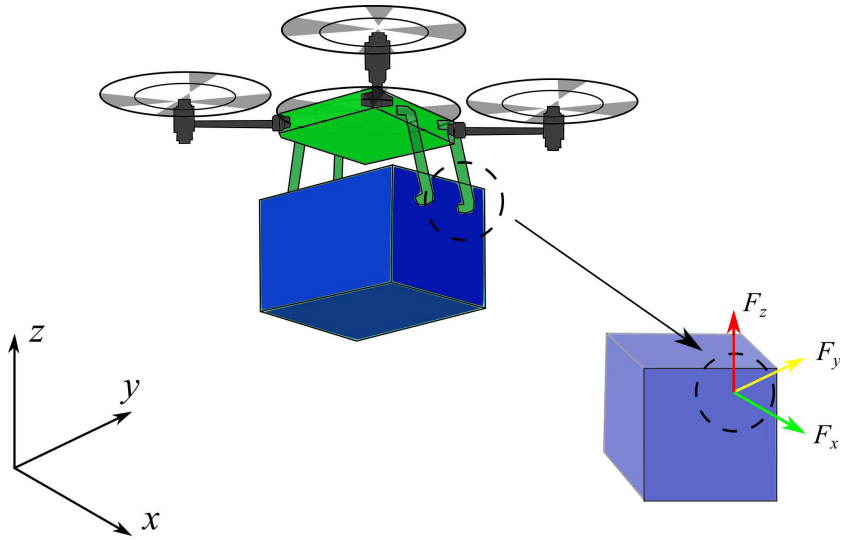

Figure 1. Schematic illustration of the UAV carrying a payload, where F_x, F_y and F_z are the elastic forces that connect the quadcopter and its payload.

The general equation of motion for the quadcopter carrying a payload is defined in the inertial reference frame, and it is represented by Eq. (1) as:

$$\mathbf{M}_\eta \ddot{\boldsymbol{\eta}} + \mathbf{C}_\eta \dot{\boldsymbol{\eta}} + \mathbf{K}_\eta \boldsymbol{\eta} + \mathbf{g}_\eta = \boldsymbol{\tau}_\eta + \mathbf{F}_d \tag{1}$$

where $\mathbf{M}_\eta$ is the inertial matrix, $\mathbf{C}_\eta$ represents the Coriolis matrix, $\mathbf{K}_\eta$ is the stiffness matrix, $\mathbf{g}_\eta$ is the gravitational vector, $\boldsymbol{\tau}_\eta$ denotes the control torque vector, $\boldsymbol{\eta}$ is the generalized coordinate vector, and $\mathbf{F}_d$ is the external disturbance

applied to the system. The matrices of Eq. (1) can also be represented in the body-fixed reference, yielding:

$$\begin{aligned}
&\mathbf{M}_\eta = \mathbf{I}_{9\times 9} \\
&\mathbf{C}_\eta = \mathbf{J}_p\mathbf{M}_p^{-1}\mathbf{C}_p\mathbf{J}_p^{-1} - \dot{\mathbf{J}}_p\mathbf{J}_p^{-1} \\
&\mathbf{K}_\eta = \mathbf{J}_p\mathbf{M}_p^{-1}\mathbf{K}_p \\
&\mathbf{g}_\eta = \mathbf{J}_p\mathbf{M}_p^{-1}\mathbf{g}_{0p} \\
&\boldsymbol{\tau}_\eta = \mathbf{J}_p\mathbf{M}_p^{-1}\boldsymbol{\tau}
\end{aligned} \tag{2}$$

where $\mathbf{I}_{9\times 9}$ is the identity matrix, $\mathbf{J}_p$ is the transformation matrix, and $\dot{\mathbf{J}}_c$ is the derivative of the transformation matrix with respect to time. For convenience, the inertial matrix in the body-frame $\mathbf{M}_p$ is defined as:

$$\mathbf{M}_p = diag(m, m, m, I_{xx} + I_{xx}^p, I_{yy} + I_{yy}^p, I_{zz} + I_{zz}^p, m_p, m_p, m_p) \tag{3}$$

where m is the quadcopter mass, m_p is the payload weight, and I_{ii} and I_{ii}^p (where $ii = x, y, z$) are the moments of inertia related to the quadcopter and its attached mass, respectively. The Coriolis matrix $\mathbf{C}_p$ is expressed as follows:

$$\mathbf{C}_p = \begin{bmatrix} m\mathbf{C}_{p1} & \mathbf{0}_{3\times 3} & \mathbf{0}_{3\times 3} \\ \mathbf{0}_{3\times 3} & \mathbf{C}_{p2} & \mathbf{0}_{3\times 3} \\ \mathbf{0}_{3\times 3} & \mathbf{0}_{3\times 3} & m_p\mathbf{C}_{p1} \end{bmatrix} \tag{4}$$

where:

$$\mathbf{C}_{p1} = \begin{bmatrix} 0 & -\omega_z & \omega_y \\ \omega_z & 0 & -\omega_x \\ -\omega_y & \omega_x & 0 \end{bmatrix} \qquad \mathbf{C}_{p2} = \begin{bmatrix} 0 & 0 & I_1\omega_y \\ I_2\omega_z & 0 & 0 \\ 0 & I_3\omega_x & 0 \end{bmatrix} \tag{5}$$

where ω_x, ω_y and ω_z are the angular velocities of the quadcopter, I_1, I_2, I_3 are the moments of inertia along x, y, z axes, and they are defined as $I_1 = (I_{zz} + I_{zz}^p) - (I_{yy} + I_{yy}^p)$, $I_2 = (I_{xx} + I_{xx}^p) - (I_{zz} + I_{zz}^p)$ and $I_3 = (I_{yy} + I_{yy}^p) - (I_{xx} + I_{xx}^p)$. The $\mathbf{0}_{a\times b}$ are zero matrices with a rows and b columns. The elastic constraint force ($F_i = k_p(i_p - i)$, where $i = x, y, z$) between the quadcopter and its payload can also be represented by a stiffness matrix, given by:

$$\mathbf{K}_p = \begin{bmatrix} \mathbf{K}_{pm} & \mathbf{0}_{3\times 3} & -\mathbf{K}_{pm} \\ \mathbf{0}_{3\times 3} & \mathbf{0}_{3\times 3} & \mathbf{0}_{3\times 3} \\ -\mathbf{K}_{pm} & \mathbf{0}_{3\times 3} & \mathbf{K}_{pm} \end{bmatrix} \tag{6}$$

where $\mathbf{K}_{pm}$= diag(k_p, k_p, k_p), such that k_p is the component related to the spring along its direction, and $diag(.)$ represents a diagonal matrix. The transformation matrix for the proposed model is defined by $\mathbf{J}_p$, which is a diagonal matrix $(\mathbf{J}_{p1}, \mathbf{J}_{p2}, \mathbf{J}_{p1})$, yielding:

$$\mathbf{J}_{p1} = \begin{bmatrix} c\psi c\theta & s\phi s\theta c\psi - c\phi s\psi & c\phi s\theta c\psi + s\psi s\phi \\ s\psi c\theta & s\phi s\theta s\psi + c\phi c\psi & c\phi s\theta s\psi - s\phi c\psi \\ -s\theta & s\phi c\theta & c\phi c\theta \end{bmatrix} \qquad \mathbf{J}_{p2} = \begin{bmatrix} 1 & s\phi t\theta & c\phi t\theta \\ 0 & c\phi & -s\phi \\ 0 & s\phi/c\theta & c\phi/c\theta \end{bmatrix} \tag{7}$$

where $s(.)$ and $c(.)$ represent the sine and cosine functions. The gravitational vector is represented by $\mathbf{g}_{0p} = \{-mgs\theta \;\; mgc\theta s\phi \;\; mgc\theta c\phi \;\; 0 \;\; 0 \;\; 0 \;\; -m_c gs\theta \;\; m_c gc\theta s\phi \;\; m_c gc\theta c\phi\}^T$. The external disturbance force is applied vertically, which is defined by a sine function as $\mathbf{F}_d = 2 * sin(\omega t)$. Additionally, the second order differential motion equation (Eq. 1) can also be represented in the state space form as follows:

$$\dot{\boldsymbol{x}}_s(t) = \mathbf{A}_c\boldsymbol{x}_s(t) + \mathbf{B}\mathbf{u}(t) + \mathbf{X}_{gc} - \mathbf{B}_{Sf}\mathbf{K}_{Sf}\boldsymbol{x}(t) \tag{8}$$

where the state vector is $\boldsymbol{x}_s = \{\dot{\boldsymbol{\eta}} \quad \boldsymbol{\eta}\}^T$, the input control $\mathbf{u}(t) = \{\boldsymbol{\tau}_\eta \quad \mathbf{0}_{9\times 1}\}^T$, $\mathbf{X}_{\eta c} = \{-\mathbf{M}_\eta^{-1}\mathbf{g}_\eta \quad \mathbf{0}_{9\times 1}\}^T$ is the gravitational vector, and the expression $\mathbf{B}_{Sf}\mathbf{K}_{Sf}\boldsymbol{x}(t)$ is related to the State-Feedback Control. The generalized coordinates vector of the quadcopter in inertial reference frame is given by $\boldsymbol{\eta} = \{x \;\; y \;\; z \;\; \phi \;\; \theta \;\; \psi \;\; x_p \;\; y_p \;\; z_p\}^T$, where x, y, z and ϕ, θ, ψ are the positions and orientation angles of the quadcopter, while x_p, y_p, z_p are the payload positions. The dynamic ($\mathbf{A}_c$) and input matrices ($\mathbf{B}$) are respectively defined as:

$$\mathbf{A}_c = \begin{bmatrix} -\mathbf{M}_\eta^{-1}\mathbf{C}_\eta & -\mathbf{M}_\eta^{-1}\mathbf{K}_\eta \\ \mathbf{I}_{9\times 9} & \mathbf{0}_{9\times 9} \end{bmatrix} \qquad \mathbf{B} = \begin{bmatrix} \mathbf{M}_\eta^{-1} \\ \mathbf{0}_{9\times 9} \end{bmatrix} \tag{9}$$

3. CONTROL DESIGN

The controller design is composed of two sub-sections i) Sliding Mode Control, ii) State-Feedback Control. The non-linear control (SMC) is used to calculate the input vector and then ensure that the quadcopter follows the desired trajectory. The linear control H_∞ (based on the mass-spring approximation) is designed to reduce the payload relative displacement, providing lower vibration amplitudes on the payload in comparison to the absence of the controller.

Concerning on experimental trails, H_∞ can be represented by a piezoelectric stack actuator, which is able to cover a wide range of frequency. In addition, several flight controllers are available to design the SMC, such as the open-source Pixhwalk, APM, and others. The experiments might be carried out at LARCASE laboratory, where presents several simulators, wind tunnels and UAV prototypes Botez (2018).

3.1 Sliding Mode Control

The SMC is divided into two subsystems: fully ($\ddot{z}$,$\ddot{\psi}$), and under actuated ($\ddot{x}$, $\ddot{y}$, $\ddot{\phi}$, $\ddot{\theta}$) subsystems. The current state variables $[z, \psi]$ must converge to the desired state variables $[z_{des}, \psi_{des}]$. Firstly, The sliding surface must be chosen to determine the UAV dynamics. Considering the axis z, it can be written as Sudhir and Swamp (2016):

$$s_z = \lambda_z(z_{des} - z) + (\dot{z}_{des} - \dot{z}) \tag{10}$$

where λ_z is a closed loop bandwidth parameter, z_{des}, z are the desired and current vertical states, and $\dot{z}_{des}, \dot{z}$ are their derivatives with respect to time. The derivative of the sliding surface is calculated as $\dot{s}_z = \lambda_z(\dot{z}_{des} - \dot{z}) + (\ddot{z}_{des} - \ddot{z})$. Time derivative of s_i can also be defined by a discontinuous state function to enforce the proposed controller strongly on the surface Utkin (2013), yielding:

$$\dot{s}_i = -\epsilon_i sat(s_i) - \eta_i s_i \tag{11}$$

where ϵ_i and η_i are the sliding surface exponential approach coefficients. Combining time derivative ($\dot{s}_z$), the state function ($\dot{s}_i$) and motion equations in z and z_p directions (defined in App. A), the corresponding control law is expressed as Zheng *et al.* (2014):

$$U_1 = \frac{\tilde{m}}{c\theta c\phi}(\epsilon_z sat(s_z) + \eta_z s_z + \lambda_z(\dot{e}_z) + \ddot{z}_{des} + g) \tag{12}$$

For the proposed configuration, the SMC must be able to lift the quadcopter and its payload, such that $\tilde{m} = m + m_c$. Additionally, the error $\dot{e}_z$ is the difference between the desired and current state variable ($\dot{z}_{des} - \dot{z}$), while $sat(.)$ is the saturated function, used to alleviate the effect of chattering on the actuators Vahdanipour and Khodabandeh (2019). This function is defined by $sat(s_i) = s_i/(|s_i| + \gamma)$, where γ is a parameter used to represent the transition bandwidth. To enable the quadcopter motion in the x, y plane, the desired roll and pitch angles (ϕ_{des}, θ_{des}) are generated through two virtual inputs, since they are directly dependent. The desired references for designing the attitude control are obtained as follows:

$$\phi_{des} = sin^{-1}(u_x s\psi - u_y c\psi) \qquad \theta_{des} = sin^{-1}\left(\frac{u_x c\psi + u_y s\psi}{c\psi}\right) \tag{13}$$

where u_x and u_y are defined by $u_x = \frac{\tilde{m}}{U_1}[\ddot{x}_{des} + \lambda_x \dot{e}_x + \eta_x s_x + \epsilon_x sat(s_x)]$ and $u_y = \frac{\tilde{m}}{U_1}[\ddot{y}_{des} + \lambda_y \dot{e}_y + \eta_y s_y + \epsilon_y sat(s_y)]$, such that λ_x, λ_y, η_x, η_y, ϵ_x and ϵ_y are positive real constants. Likewise, U_2, U_3 and U_4 are designed combining the motion equation for its respective axis, time derivative ($\dot{s}_i$), and the state function (Eq. 11), yielding:

$$\begin{aligned}
U_2 &= \tfrac{I_{xx}}{l}[\ddot{\phi}_{des} + \lambda_\phi \dot{e}_\phi + \eta_\phi s_\phi + \epsilon_\phi sat(s_\phi)] - (I_{yy} - I_{zz}) l\dot{\theta}\dot{\psi} \\
U_3 &= \tfrac{I_{yy}}{l}[\ddot{\theta}_{des} + \lambda_\theta \dot{e}_\theta + \eta_\theta s_\theta + \epsilon_\theta sat(s_\theta)] - (I_{zz} - I_{xx}) l\dot{\phi}\dot{\psi} \\
U_4 &= I_{zz}[\ddot{\psi}_{des} + \lambda_\psi(\dot{e}_\psi) + \eta_\psi s_\psi + \epsilon_\psi sat(s_\psi)] - (I_{xx} - I_{yy})\dot{\theta}\dot{\phi}
\end{aligned} \tag{14}$$

where λ_ϕ, λ_θ, λ_ψ, ϵ_ϕ, ϵ_θ, ϵ_ψ, η_ϕ, η_θ and η_ψ are positive real constant parameters. Additionally, the input control vector is defined by:

$$\boldsymbol{\tau} = \{0\ 0\ U_1\ U_2\ U_3\ U_4\ 0\ 0\ 0\}^T \tag{15}$$

As a theoretical work, all the states were calculated using the equations of motion. However, the quadcopter and its payload states can be measured using three axial sensors in numerical trials. All the steps required for stability proof can be found in Zheng *et al.* (2014).

3.2 State-Feedback Control H_∞

The State-Feedback Control H_∞ is developed to suppress the residual payload vibration. The dynamics of 2-DOF mass-spring is used to design the proposed control law instead of considering the full equations of motion. This simplification aims to evaluate the use of a linear controller performance in reducing the payload displacement. App. A presents the complimentary details of the simplifications. Fig. 2 depicts the schematic illustration of the UAV carrying a payload.

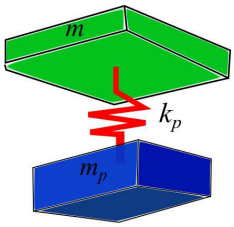

Figure 2. Schematic illustration of the UAV carrying a payload, where m is the UAV mass, m_p is the mass of the payload, and k_p represents the coupling stiffness.

The State Feedback control is initially applied to the vertical direction, however, it can be extended to other axes. The equations of motion for the mass-spring, considering an input U_1 acting on the main mass m, are represented as follows:

$$\begin{bmatrix} m & 0 \\ 0 & m_p \end{bmatrix} \begin{Bmatrix} \ddot{z} \\ \ddot{z}_p \end{Bmatrix} + \begin{bmatrix} k_p & -k_p \\ -k_p & k_p \end{bmatrix} \begin{Bmatrix} z \\ z_p \end{Bmatrix} = \begin{Bmatrix} 1 \\ 0 \end{Bmatrix} U_1 \tag{16}$$

or represented in a state space form $\dot{\boldsymbol{x}}_s = \mathbf{A}_s \boldsymbol{x}_s + \mathbf{B}_s U_1$, where $\mathbf{A}_s$ is the dynamic matrix, $\mathbf{B}_s$ is the control matrix, and $\boldsymbol{x}_s$ is the state vector. Lyapunov's method is used to study the stability of solutions of the investigated equation applied to high order systems, represented by $\mathbf{V}(\boldsymbol{x}_s) = \boldsymbol{x}_s^T \mathbf{P} \boldsymbol{x}_s$. Lyapunov function must be positive definite, while its derivative is semi-definite negative. Using the mass-spring state-form representation and applying the feedback control as $U_1 = -\mathbf{K}_h \boldsymbol{x}_s$, where $\mathbf{K}_h$ is the gain matrix, the generic equation with decay rate α is represented as Linear Matrix Inequality (LMI):

$$\mathbf{W}\mathbf{A}_s^T + \mathbf{A}_s\mathbf{W} - \mathbf{Z}^T\mathbf{B}_s^T - \mathbf{B}_s\mathbf{Z} + 2\alpha\mathbf{W} < \mathbf{0} \tag{17}$$

In addition, to ensure a minimum decay rate α, damping ratio $\xi = cos(\theta_h)$, and minimum undamped natural frequency $\omega_d = r sin(\theta_h)$, the poles must be calculated in a specific region of interest as shown in Fig. 3.

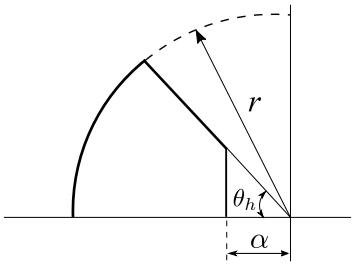

Figure 3. Region $S(\alpha, r, \theta_h)$. Adapted from Chilali and Gahinet (1996).

For convenience, only the upper region part is represented, since it is symmetric. The theorem provides the following LMI characterization for $S(\alpha, r, \theta_h)$, in which:

$$\begin{bmatrix} -r\mathbf{W} & \mathbf{A}_s\mathbf{W} - \mathbf{B}_s\mathbf{Z} \\ \mathbf{W}\mathbf{A}_s - \mathbf{Z}^T\mathbf{B}_s^T & -r\mathbf{W} \end{bmatrix} < \mathbf{0} \tag{18}$$

$$\begin{bmatrix} sin\theta_h(\mathbf{W}\mathbf{A}_s^T + \mathbf{A}_s\mathbf{W} - \mathbf{Z}^T\mathbf{B}_s^T - \mathbf{B}_s\mathbf{Z}) & cos\theta_h(-\mathbf{W}\mathbf{A}_s^T + \mathbf{A}_s\mathbf{W} + \mathbf{Z}^T\mathbf{B}_s^T - \mathbf{B}_s\mathbf{Z}) \\ cos\theta_h(\mathbf{W}\mathbf{A}_s^T - \mathbf{A}_s\mathbf{W} - \mathbf{Z}^T\mathbf{B}_s^T + \mathbf{B}_s\mathbf{Z}) & sin\theta_h(\mathbf{W}\mathbf{A}_s^T + \mathbf{A}_s\mathbf{W} - \mathbf{Z}^T\mathbf{B}_s^T - \mathbf{B}_s\mathbf{Z}) \end{bmatrix} < \mathbf{0} \tag{19}$$

Then, combining Eqs. (17), (18), and (19), it is possible to calculate the poles of the LMI, restricting to the three elementary regions: an α stability, a disk, and a conic sector. Following these conditions, the gain matrix is calculated by $\mathbf{K}_h = \mathbf{Z}\mathbf{W}^{-1}$. According to Eq. (8), the matrices are defined by $\mathbf{B}_{Sf} = \{\mathbf{0}_{8x1} \quad 1 \quad \mathbf{0}_{9x1}\}$, and $\mathbf{K}_{Sf} = \{\mathbf{0}_{8x1} \quad \mathbf{K}_h \quad \mathbf{0}_{9x1}\}^T$,in which are applied in the vertical degree of freedom for the payload (in order to cancel the attachment force F_z, as seen in Fig. 1). The expression $\mathbf{K}_h$ represents the second gain term of the matrix for the mass-spring model.

4. RESULTS AND DISCUSSION

The physical properties of the quadcopter carrying a payload are presented in Tab. 1, and the controller gains of the SMC are listed in Tab. 2. All the initial states are considered zero, except for $\psi = 0.5rad$.

Table 1. Physical and geometric properties of the quadcopter.

Property	m	k_p	l	I_{xx}	I_{yy}	I_{zz}
Value	1.350	103.40	0.1750	0.0167	0.0167	0.0231
Unit	kg	N/m	m	kgm^2	kgm^2	kgm^2

Table 2. Controller gains computed for the SMC.

Parameter	**Value**	**Parameter**	**Value**
ϵ_x, ϵ_y, ϵ_z,	2.20, 1.80, 1.80	ϵ_ϕ, ϵ_θ, ϵ_ψ,	1.50, 1.10, 1.10
λ_x, λ_y, λ_z	3.00, 3.20, 3.20	λ_ϕ, λ_θ, λ_ψ	1.50, 1.50, 1.50
η_x, η_y, η_z	0.40, 0.40, 0.40	η_ϕ, η_θ, η_ψ, γ	0.04, 0.04, 0.04, 0.20

The SMC is used to perform the desired trajectory, in which is composed of four main phases: i) taking-off, ii) cruise phase at altitude 1, iii) cruise phase at altitude 2 (higher than the first one), and iv) the landing phase. Both cruise phases are performed along the x axis, while in the y there is a slightly displacement during the flight. The indices $\bar{X}$, $\bar{Y}$, $\bar{Z}$ are the dimensionless axes, such that $x(t)/x_{max}$, $y(t)/y_{max}$, and $z(t)/z_{max}$, respectively. In addition, $x(t), y(t), z(t)$ are the trajectory displacements of the UAV, and $x_{max}, y_{max}, z_{max}$ are the maximum displacement achieved by the UAV along its respective axis, and the coefficient τ_t is defined by the ratio of t/t_{max}.

It is assumed an elastic link (represented by stiffness) between the quadcopter and its payload, allowing the payload to translate along all directions (x, y and z). Thereby, this relative displacements are used to evaluate their influence on both sub-systems. They are defined by the difference between the payload and the quadcopter trajectories, such as $R_{dx} = x_p - x$. Figure 4 shows the three dimensional trajectory of the quadcopter with an attached mass, and the relative displacement represented along the x, y and z.

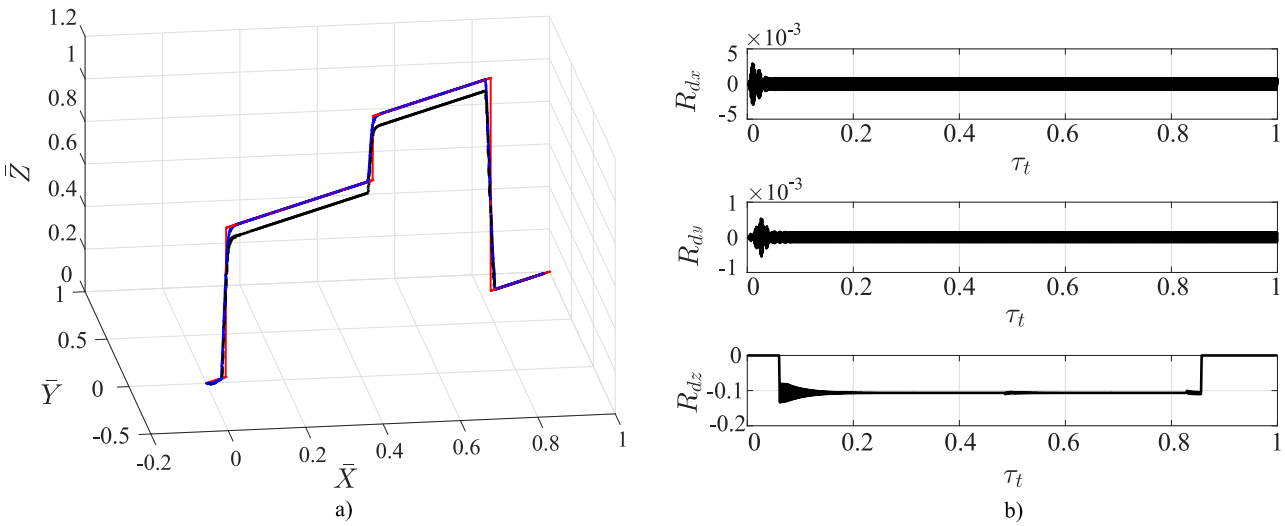

Figure 4. Three dimensional trajectory of the quadcopter carrying a payload, where desired (solid red line −), quadcopter trajectory (solid blue line −), payload (dash-dotted black line −.), and relative displacement (solid black line −).

The vertical component presents the most significant percentage of the relative displacement, exhibiting more promi-

nent peaks especially during maneuvers (as seen in Fig. 4). Based on this flight, it is important to evaluate the effect of sudden acceleration on the quadcopter and payload trajectories, represented by change of altitude. The relative displacement between them might cause unwanted vibration to the transported load, and depending on its amplitude, hazardous interference can be related. Figure 5 depicts the vertical trajectory component and the difference of the quadcopter and its payload trajectories.

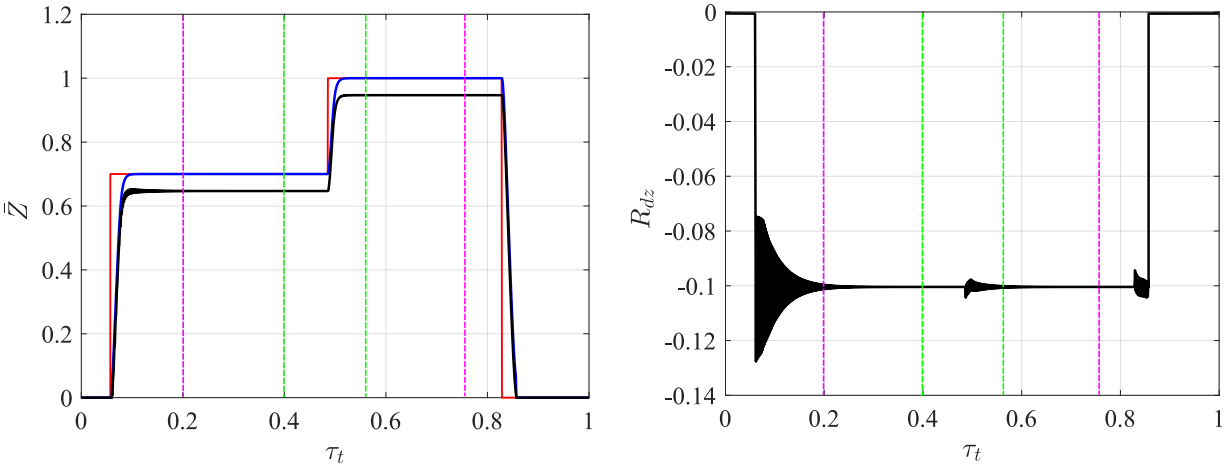

Figure 5. Flight behavior a) vertical trajectory b) Relative displacement, where desired (solid red line $-$), quadcopter trajectory (solid blue line $-$), and payload (dash-dotted black line $-.$), relative displacement (solid black line $-$), and boundaries of the flight are represented by dashed black $--$ and magenta $--$ lines.

Additionally, in the presence of external disturbances, the relative displacement can be significantly increased, reducing the system performance. Then, an external disturbance is applied vertically to the system during the interval $0.42 < \tau_t < 0.72$, limited by two dashed yellow lines $--$. Figure 6 shows the influence of the presence and the absence of external disturbance.

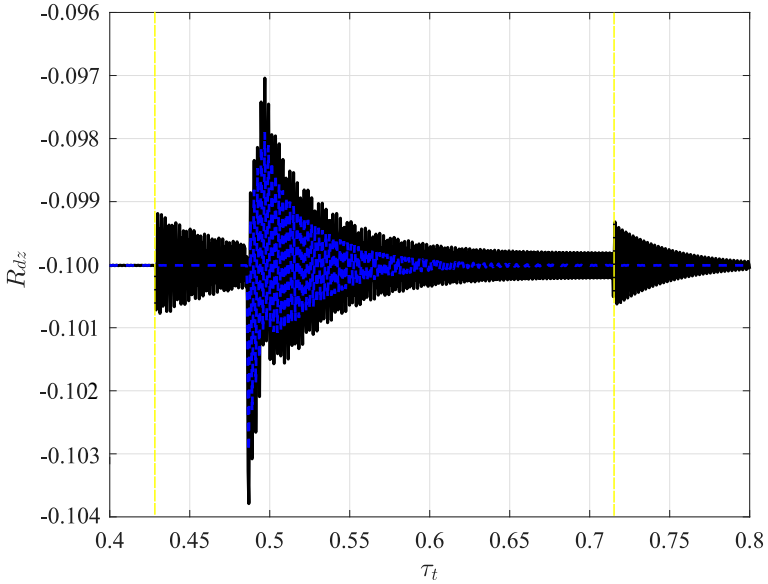

Figure 6. Effect of external disturbance on the relative oscillation, where in the absence (dashed blue line $--$), and in the presence (solid black line $-$) of external disturbance.

It is worth mentioning that a higher value of R_{dz} represents a more significant force (F_z) that impacts on the payload. The Parseval's theorem is used to evaluate the sum of energy originated from the quadcopter and payload trajectories, and then estimate a metric of comparison. Consider the Parseval's theorem, defined in time:

$$P_i = \int_{i=1}^{N} |dp_i^2(t)|dt \tag{20}$$

where P_i the Parseval coefficient, N is the vector length, and dp_i is the analyzed state along the x, y and z. According to the Parseval theorem, it is possible to verify amplification of 30% of the relative displacement (R_{dz}), when the UAV is subjected to external disturbances. This increase of relative displacement, i.e. unwanted vibration, must decrease the payload integrity and the quadcopter performance. Figure 7 depicts the influence of the State-Feedback control in attenuating the relative displacements.

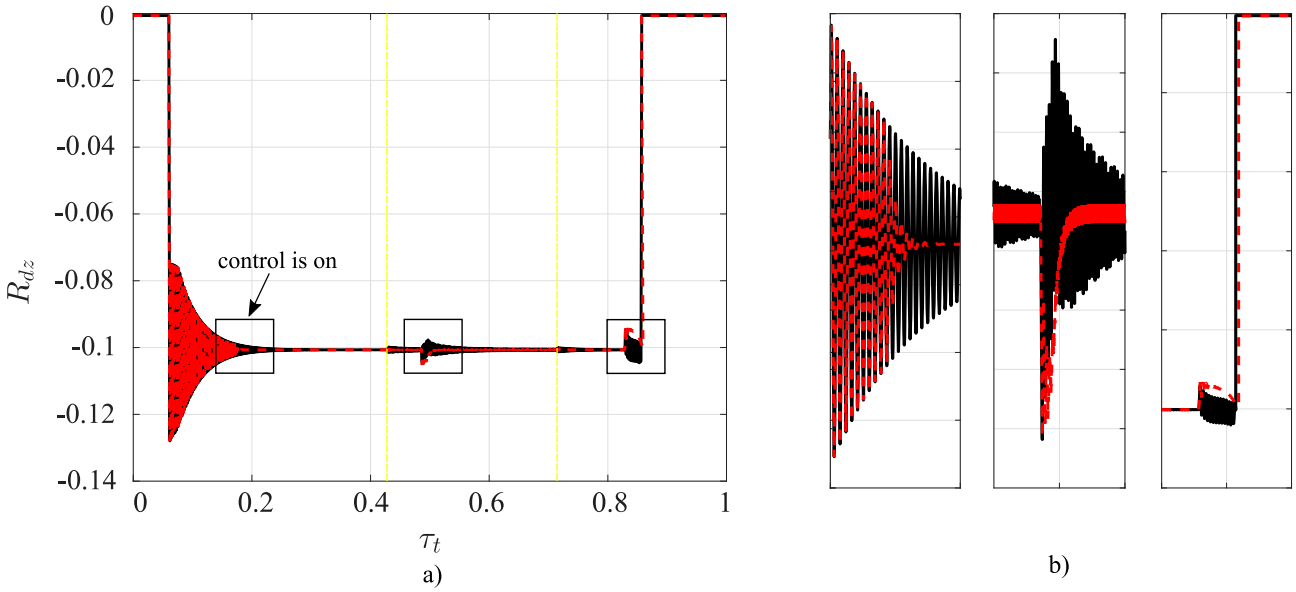

Figure 7. State-Feedback Control on the relative displacement behavior, where a) vertical relative displacement b) zoom boxes of a), where absence of control (solid black line $-$), and presence of control (dashed red line $--$).

Then, in the presence of the State-Feedback Control, the oscillations are decreased, and consequently the forces that impact the payload are reduced. According to the presented results, the presence of the State-Feedback control reduced the vibrations amplitudes in comparison to the uncontrolled case. In terms of Parseval coefficient, a reduction of almost 50% is related to the second analyzed interval. As already mentioned, based on the flight configuration and numerical results, the controller is restrictively applied to the z axis, since it presents the most significant force impacting on the payload. However, it can also be extended to other directions.

5. FINAL REMARKS

The UAV's ability to carry payload has conquered attention to different areas, such as medical transportation, environmental monitoring, and more recently to food delivery. Some medical products require a smoother flight, that is, with smaller vibration magnitude. Pilot maneuvers and external disturbances might increase the undesired vibration on the payload due to the direct connection between the UAV and its payload, impacting the signal accuracy from on-board components as well as the payload quality.

Based on the results, all directions presented a residual relative displacement during the flight, increasing the unwanted vibration on the payload, and then decreasing the UAV performance. The vertical component exhibited a more significant influence on the system for the proposed flight configuration, since higher amplitude peaks are presented. The combination of the SMC and the State-Feedback can attenuate the external disturbance and excessive vibration influences, alleviating the energy transferred from the quadcopter to its payload. Therefore, the use of the State-Feedback combined with the SMC reduces the constraint force (between the UAV and its payload) and the undesired vibration by almost 50% than the case with no presence of the H_∞.

ACKNOWLEDGEMENTS

The first author would like to thanks to the Brazilian Coordination for the Improvement of Higher Education Personnel (CAPES)- Finance Code 001 for his scholarship. The second author thanks to the NSERC for the Canada Research Chair Holder Tier 1 in Aircraft Modeling and Simulation Technologies Program. The third author gives special thanks to the National Council for Scientific and Technological Development (CNPq) Grant no. 429963/2016-5 for its financial support.

REFERENCES

Alkomy, H. and Shan, J., 2021. "Vibration reduction of a quadrotor with a cable-suspended payload using polynomial trajectories". *Nonlinear Dynamics*, pp. 1–23.

Aouf, N., Boulet, B. and Botez, R., 2000. "Robust gust load alleviation for a flexible aircraft". *Canadian Aeronautics and Space Journal*, Vol. 46, No. 3, pp. 131–139.

Botez, R., 2018. "Morphing wing, uav and aircraft multidisciplinary studies at the laboratory of applied research in active controls, avionics and aeroservoelasticity larcase". *Aerospace Lab*, , No. 14, pp. 1–11.

Chilali, M. and Gahinet, P., 1996. "h_∞ design with pole placement constraints: An lmi approach". *IEEE TRANSACTIONS ON AUTOMATIC CONTROL*, Vol. 41, pp. 1–10.

Dancila, R.I. and Botez, R.M., 2021. "New atmospheric data model for constant altitude accelerated flight performance prediction calculations and flight trajectory optimization algorithms". *Proceedings of the Institution of Mechanical Engineers, Part G: Journal of Aerospace Engineering*, Vol. 235, No. 4, pp. 405–426.

Fossen, T.I., 1999. "Guidance and control of ocean vehicles".

Ghazi, G., Botez, R.M., Bourrely, C. and Turculet, A.A., 2021. "Method for calculating aircraft flight trajectories in presence of winds". *Journal of Aerospace Information Systems*, pp. 1–22.

Gobeaut, J., Couffignal, M., Boely, N., Bourgeteau, Q., Mareschal, N., Botez, R. and Triandaf, I., 2009. "Methods of modeling of an underwater unmanned vehicle (uuv)". In *AIAA Guidance, Navigation, and Control Conference*. p. 5981.

Hampson, M., 2018. "Drone delivers human kidney: The organ was flown several kilometers by a drone without incurring damage-[news]". *IEEE Spectrum*, Vol. 56, No. 1, pp. 7–9.

Hii, M.S.Y., Courtney, P. and Royall, P.G., 2019. "An evaluation of the delivery of medicines using drones". *Drones*, Vol. 3, No. 3, p. 52.

Kammegne, M.J.T., Botez, R.M., Grigorie, L.T., Mamou, M. and Mébarki, Y., 2017. "Proportional fuzzy feed-forward architecture control validation by wind tunnel tests of a morphing wing". *Chinese Journal of Aeronautics*, Vol. 30, No. 2, pp. 561–576.

Kuitche, M.A.J. and Botez, R.M., 2019. "Modeling novel methodologies for unmanned aerial systems–applications to the uas-s4 ehecatl and the uas-s45 bálaam". *Chinese Journal of Aeronautics*, Vol. 32, No. 1, pp. 58–77.

Rahmani, F., Rahmani, R., Mobayen, S. and Fekih, A., 2021. "Lmi-based state feedback design for quadcopter optimal path control and tracking". In *2021 American Control Conference (ACC)*. IEEE, pp. 4655–4659.

Sudhir and Swamp, A., 2016. "Second order sliding mode control for quadrotor". In *2016 IEEE First International Conference on Control, Measurement and Instrumentation (CMI)*. pp. 92–96. doi:10.1109/CMI.2016.7413717.

Utkin, V.I., 2013. *Sliding modes in control and optimization*. Springer Science & Business Media,.

Vahdanipour, M. and Khodabandeh, M., 2019. "Adaptive fractional order sliding mode control for a quadrotor with a varying load". *Aerospace Science and Technology*, Vol. 86, pp. 737–747.

Yakushiji, K., Yakushiji, F. and Fujita, H., 2020. "The quality of blood dropped from an unmanned aerial vehicle (drone)". *Hematol. Transfus. Int. J*, Vol. 8, pp. 38–40.

Yañez-Badillo, H., Beltran-Carbajal, F., Tapia-Olvera, R., Kuitche, M. and Botez, R., 2019a. "Generalized extended state observer based-control for active suppression of forced vibrations in a multi-rotor unmanned vehicle".

Yañez-Badillo, H., Botez, R., Kuitche, M., Beltran-Carbajal, F. and Tapia-Olvera, R., 2019b. "Integral compensation for disturbance rejection in longitudinal flight control of a fixed-wing unmanned aerial system".

Zheng, E.H., Xiong, J.J. and Luo, J.L., 2014. "Second order sliding mode control for a quadrotor uav". *ISA transactions*, Vol. 53, No. 4, pp. 1350–1356.

RESPONSIBILITY NOTICE

The authors are solely responsible for the printed material included in this paper.

A Simplified Equations

The equations of the motion carrying a payload are represented in Eq. (1) at hovering condition. The UAV motion equations for the vertical axis can be simplified, and the following equations are obtained as:

$$\begin{aligned} m\ddot{z} &= -mg - k_p(z - z_p) + U_1 \\ m_p\ddot{z}_p &= -m_p g + k_p(z - z_p) \end{aligned} \tag{21}$$

The controller design for vibration suppression can neglect the gravitational term. Then, Eq. (21) can be rewritten as a 2-DOF mass-spring system.